

Constrained Radar Waveform Design for Range Profiling

Bo Tang, Jun Liu, *Senior Member, IEEE*, Hai Wang, and Yihua Hu

Abstract

Range profiling refers to the measurement of target response along the radar slant range. It plays an important role in automatic target recognition. In this paper, we consider the design of transmit waveform to improve the range profiling performance of radar systems. Two design metrics are adopted for the waveform optimization problem: one is to maximize the mutual information between the received signal and the target impulse response (TIR); the other is to minimize the minimum mean-square error for estimating the TIR. In addition, practical constraints on the waveforms are considered, including an energy constraint, a peak-to-average-power-ratio constraint, and a spectral constraint. Based on minorization-maximization, we propose a unified optimization framework to tackle the constrained waveform design problem. Numerical examples show the superiority of the waveforms synthesized by the proposed algorithms.

Index Terms

Range profiling, waveform optimization, constrained design, minorization-maximization (MM).

Bo Tang, Hai Wang, and Yihua Hu are with the College of Electronic Engineering, National University of Defense Technology, Hefei 230037, China (email: tangbo06@gmail.com; wanghai17@nudt.edu.cn; yh_hu@263.net).

Jun Liu is with the Department of Electronic Engineering and Information Science, University of Science and Technology of China, Hefei, China (email: jun_liu_math@hotmail.com).

This work of Bo Tang was supported in part by the National Natural Science Foundation of China under Grant 61671453 and 61801500, in part by the Young Elite Scientist Sponsorship Program under Grant 17-JCJQ-QT-041, and in part by the Anhui Provincial Natural Science Foundation under Grant 1908085QF252.

The work of Jun Liu was supported in part by the National Natural Science Foundation of China under Grant 61871469 and in part by the Youth Innovation Promotion Association of the Chinese Academy of Sciences under Grant CX2100060053.

The work of Yihua Hu was supported in part by the National Natural Science Foundation of China under Grant 61871389 and in part by the Research Plan Project of the National University of Defense Technology under Grant ZK18-01-02.

arXiv:2103.10320v1 [eess.SP] 18 Mar 2021

I. INTRODUCTION

Radar range profiling refers to the generation of high resolution range profiles (HRRP) by processing the target returns. The generated HRRP can be used for image formation [1] and automatic target recognition [2] in radar systems. Conventional wideband radar systems usually transmit high-range-resolution waveforms (e.g., the linear frequency-modulated (LFM) waveforms, also called chirp waveforms) and use matched filtering (MF) to obtain range profiles. However, the optimality of transmitting such waveforms is not guaranteed. Moreover, it is well-known that the MF is optimal only in the sense of maximizing signal-to-noise-ratio (SNR) for point-like target detection in the presence of white noise.

Essentially, radar range profiling is a process of extracting information from target echoes. It can also be viewed as a parameter estimation problem, where the target impulse response (TIR) is the parameter of interest. Therefore, estimators other than the MF can be used to improve the range profiling performance. Well-known data-independent estimators include mismatched filter (MMF) and least-square (LS) estimator (see, e.g., [3]–[5] and the references therein). The MMF improves the signal-to-clutter-plus-noise ratio (SCNR) but suffers some SNR loss. In [6], the authors pointed out that, an improper selection of the processing window for the LS estimator degraded the range profiling performance. To overcome the limitation of the LS estimator, they proposed a data adaptive approach, called adaptive pulse compression (APC). The APC algorithm achieved low estimation errors and was capable of unmasking weak targets. In [7], this algorithm was tested on measured data and showed the superiority over the conventional MF. Moreover, if the TIR is sparse (i.e., the number of non-zero component of the TIR is small), algorithms based on sparse reconstruction can be applied to estimate the TIR (see, e.g., [8] and the references therein).

In addition to deriving estimators (in the receiver), there are also considerable interests in designing waveforms (in the transmitter) in recent years (see, e.g., [9]–[11] and the references therein). In [12], [13], the authors proposed several computational approaches to minimize the integrated sidelobe level (ISL) of the transmit waveforms. Indeed, if MF is used in the receiver, waveforms with low ISL are useful to suppress clutter from the neighborhood range bins. Alternatively, if MMF is used, the detection performance of radar systems can be further enhanced by jointly designing the transmit waveform and receive filter (see, e.g. [14]–[18] and the references therein). However, waveforms designed for enhancing the target detection performance might not be suitable for range profiling.

For the range profiling problem, a widely used metric for designing waveforms is to maximize the mutual information between the TIR and the received signal (see, e.g., [19]–[25] and the references therein). In [19], the author derived the optimal “estimation” waveform maximizing the mutual informa-

tion. Results showed that the optimal estimation waveforms admitted a water-filling solution. In [20], the authors extended the work in [19], and proposed a waveform design algorithm for estimating multiple extended targets with a phased-array radar. In [21], the waveform design problem in the presence of signal-dependent interference was considered. In [22]–[24], radar waveform design for spectrum sharing with communication systems was addressed. However, the waveforms synthesized by the algorithms in these works are not constant-modulus, which makes them difficult to implement in practical radar systems.

In this paper, we consider the design of practically constrained waveform for range profiling with single-input-single-output (SISO) radars (which means that we extend the point-target formulation to distributed targets). Given that range profiling is a parameter estimation problem, we first consider the widely used mutual information criterion (i.e., designing waveforms based on maximizing the mutual information between the received signal and the TIR). Different from the approaches in [19]–[21], which optimized the (continuous) spectrum of the waveforms, we consider the optimization of the discrete-time waveforms. This facilitates enforcing practical constraints on the waveform. To investigate the estimation performance of the waveform designed based on mutual information maximization, we then consider the waveform design based on minimizing MMSE, and compare their performance. We develop a unified optimization framework based on minorization-maximization (MM) to tackle the encountered (non-convex) waveform design problems. Numerical examples show that the waveforms synthesized by the proposed algorithms outperform their counterparts.

The rest of this paper is organized as follows. Section II establishes the signal model and formulates the waveform design problem. Section III proposes an MM-based algorithm framework to tackle the non-convex waveform design problem. Section IV gives methods to efficiently tackle the quadratic programming problem encountered at each iteration of the proposed MM algorithms. Section V analyzes the convergence and the computational complexity of the proposed algorithms. Section VI provides numerical examples to demonstrate the performance of the proposed algorithms. Finally, we conclude the paper in Section VII.

Notations: Throughout this paper, matrices are denoted by bold uppercase letters and vectors are denoted by bold lowercase letters. $\mathbb{C}^{m \times n}$ and \mathbb{C}^k are the sets of $m \times n$ matrices and $k \times 1$ vectors with complex-valued entries. \mathbf{I} , $\mathbf{1}$, and $\mathbf{0}$ denote the identity matrix, the matrix of ones, and the matrix of zeros, with the size determined by the subscript or from the context. Superscripts $(\cdot)^T$, $(\cdot)^*$, and $(\cdot)^\dagger$ denote the transpose, the conjugate, and the conjugate transpose. The symbols $\det(\cdot)$ and $\text{tr}(\cdot)$ indicate the determinant and the trace of a square matrix. $\|\cdot\|_2$ and $\|\cdot\|_\infty$ denote the Euclidean norm and the ℓ_∞ -norm of a vector argument. $\|\cdot\|_F$ denotes the Frobenius norm of a matrix argument. \otimes and \circledast represent the Kronecker product and the operator of convolution. $\text{vec}(\mathbf{X})$ indicates the vector obtained by

column-wise stacking of the entries of \mathbf{X} . $\text{Re}(\mathbf{X})$ denotes the real part of the matrix \mathbf{X} (element-wise). $\arg(x)$ represents the argument of x . $\lfloor x \rfloor$ denotes the nearest integer less than or equal to x . The notation $\mathbf{A} \succ \mathbf{B}$ ($\mathbf{A} \succeq \mathbf{B}$) means that $\mathbf{A} - \mathbf{B}$ is positive definite (semi-definite). $\mathbf{x} \sim \mathcal{CN}(\mathbf{m}, \mathbf{R})$ means that \mathbf{x} obeys a circularly symmetric complex Gaussian distribution with mean \mathbf{m} and covariance matrix \mathbf{R} . Finally, $\mathbb{E}(x)$ denotes the expectation of the random variable x .

II. SIGNAL MODEL AND PROBLEM FORMULATION

A. Signal Model

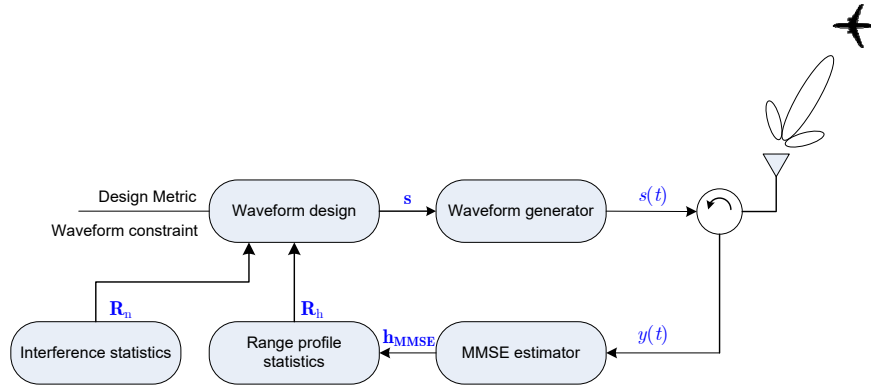


Fig. 1. Illustration of the radar system architecture.

As illustrated in Fig. 1, we consider a wideband radar system with $s(t)$ being its baseband transmit waveform. Let $h(t)$ denote the TIR. Then the down-converted received signal can be written as

$$y(t) = \int_{\tau_1}^{\tau_2} s(\tau)h(t - \tau)d\tau + n(t), \quad (1)$$

where τ_1 and τ_2 denotes the minimum and maximum two-way propagation delays, respectively, and $n(t)$ denotes the disturbance in the receiver (accounting for possible jamming signals and receiver noise). To facilitate the following discussions, we consider the discretized signal model. Let $\mathbf{s} = [s_1, s_2, \dots, s_L]^T \in \mathbb{C}^L$ denote the (discrete-time) waveform (associated with $s(t)$), and $\mathbf{h} \in \mathbb{C}^P$ denote the target response vector (associated with $h(t)$), where L is the code length, and P is the number of range cells with target signals¹. Then the digital received signal, denoted by \mathbf{y} , can be written as

$$\mathbf{y} = \mathbf{h} \otimes \mathbf{s} + \mathbf{n}, \quad (2)$$

where $\mathbf{n} \in \mathbb{C}^{L_0}$ denotes the samples corresponding to $n(t)$, and $L_0 = L + P - 1$.

¹ $P \approx B(\tau_2 - \tau_1)$, where B is the bandwidth of the signal.

Define

$$\mathbf{S} = \begin{pmatrix} s_1 & 0 & \cdots & 0 \\ s_2 & s_1 & \ddots & 0 \\ \vdots & \ddots & \ddots & 0 \\ s_L & s_{L-1} & \cdots & 0 \\ 0 & s_L & \ddots & 0 \\ \vdots & \vdots & \vdots & \vdots \\ 0 & \cdots & \cdots & s_L \end{pmatrix} \in \mathbb{C}^{L_0 \times P}. \quad (3)$$

Then \mathbf{y} can be rewritten as

$$\mathbf{y} = \mathbf{S}\mathbf{h} + \mathbf{n}. \quad (4)$$

Note that similar signal models are considered in [14], [15], [26], [27]. In these papers, the authors assumed that the TIR is known *a priori* or partially known. The assumption is justified if a template library containing TIR at all relevant target aspect angles is available, or the radar system is cognitive, i.e., the radar system can obtain the prior knowledge of the TIR from the previous estimates (see, e.g., [24], [28]–[30] and the references therein for a recent discussion). Different from [14], [15], [26], [27], which used a deterministic TIR model, we employ a stochastic TIR model. Specifically, we assume that $\mathbf{h} \sim \mathcal{CN}(\boldsymbol{\mu}_h, \mathbf{R}_h)$, where $\boldsymbol{\mu}_h$ indicates the prior knowledge of the target response and \mathbf{R}_h accounts for the uncertainty in the prior knowledge (\mathbf{R}_h can be estimated based on multiple previous estimates, or specified by the user). In addition, we assume that the disturbance \mathbf{n} obeys a Gaussian distribution with zero mean and covariance matrix \mathbf{R}_n (estimated based on target-free samples). Based on the two assumptions, we have $\mathbf{y} \sim \mathcal{CN}(\mathbf{S}\boldsymbol{\mu}_h, \mathbf{R}_s)$, where $\mathbf{R}_s = \mathbf{S}\mathbf{R}_h\mathbf{S}^\dagger + \mathbf{R}_n$.

Next we present two metrics for designing waveforms to improve the range profiling performance.

B. Waveform Design Based on Maximizing Mutual Information

The mutual information between \mathbf{y} and \mathbf{h} is given by

$$\begin{aligned} I(\mathbf{y}; \mathbf{h}) &= H(\mathbf{y}) - H(\mathbf{y}|\mathbf{h}) \\ &= \log \det(\mathbf{S}\mathbf{R}_h\mathbf{S}^\dagger + \mathbf{R}_n) - \log \det(\mathbf{R}_n) \\ &= \log \det(\mathbf{R}_n^{-1}\mathbf{S}\mathbf{R}_h\mathbf{S}^\dagger + \mathbf{I}), \end{aligned} \quad (5)$$

where $H(\mathbf{y})$ denotes the differential entropy of \mathbf{y} , and $H(\mathbf{y}|\mathbf{h})$ denotes the conditional differential entropy of \mathbf{y} given \mathbf{h} [31]. Thus, the waveform design problem based on maximizing mutual information can be formulated as follows:

$$\begin{aligned} \max_{\mathbf{s}} f_1(\mathbf{s}) &= \log \det(\mathbf{R}_n^{-1} \mathbf{S} \mathbf{R}_h \mathbf{S}^\dagger + \mathbf{I}) \\ \text{s.t. } \mathbf{s} &\in \mathcal{S}, \end{aligned} \quad (6)$$

where \mathcal{S} denotes the feasibility region of \mathbf{s} , and is determined by the constraints on the waveforms (detailed in Subsection II-D).

C. Waveform Design Based on Minimizing MMSE

Given the signal model in (4), the MMSE estimator of \mathbf{h} is given by [32]

$$\mathbf{h}_{\text{MMSE}} = \boldsymbol{\mu}_h + \mathbf{R}_h \mathbf{S}^\dagger (\mathbf{S} \mathbf{R}_h \mathbf{S}^\dagger + \mathbf{R}_n)^{-1} (\mathbf{y} - \mathbf{S} \boldsymbol{\mu}_h). \quad (7)$$

The associated MMSE is

$$\begin{aligned} \text{MMSE} &= \mathbb{E}(\|\mathbf{h} - \mathbf{h}_{\text{MMSE}}\|_2^2) \\ &= \text{tr}[(\mathbf{R}_h^{-1} + \mathbf{S}^\dagger \mathbf{R}_n^{-1} \mathbf{S})^{-1}] \\ &= \text{tr}(\mathbf{R}_h - \mathbf{R}_h \mathbf{S}^\dagger (\mathbf{S} \mathbf{R}_h \mathbf{S}^\dagger + \mathbf{R}_n)^{-1} \mathbf{S} \mathbf{R}_h), \end{aligned} \quad (8)$$

where the third equality is derived using the matrix inversion lemma [33]. Thus, the waveform design problem based on minimizing MMSE is equivalent to

$$\begin{aligned} \max_{\mathbf{s}} f_E(\mathbf{s}) &= \text{tr}(\mathbf{R}_h \mathbf{S}^\dagger (\mathbf{S} \mathbf{R}_h \mathbf{S}^\dagger + \mathbf{R}_n)^{-1} \mathbf{S} \mathbf{R}_h) \\ \text{s.t. } \mathbf{s} &\in \mathcal{S}. \end{aligned} \quad (9)$$

D. Waveform Constraints

In this paper, we consider the following constraints:

- Energy constraint. In practical radar systems, the available transmit energy for the waveform is limited. Thus, we impose the following constraint:

$$\mathbf{s}^\dagger \mathbf{s} \leq e_t, \quad (10)$$

where e_t is the total available transmit energy. It can be proved that the mutual information is increasing and the MMSE is decreasing with respect to (w.r.t.) the waveform energy (see Appendix

A for a proof). Thus, the optimal waveform maximizing the mutual information and the optimal waveform minimizing the MMSE must satisfy

$$\mathbf{s}^\dagger \mathbf{s} = e_t. \quad (11)$$

- PAPR constraint. To improve the efficiency of the radio frequency amplifier and avoid the nonlinear effect in the transmitter, waveforms with low PAPR is desired [34]–[40]. To control the PAPR of the waveform, we consider the following constraint:

$$\mathbf{s}^\dagger \mathbf{s} = e_t, \text{PAPR}(\mathbf{s}) \leq \rho, \quad (12)$$

where $1 \leq \rho \leq L$, and

$$\text{PAPR}(\mathbf{s}) = \frac{\max_l |s(l)|^2}{\frac{1}{L} \sum_{l=1}^L |s(l)|^2}. \quad (13)$$

If $\rho = 1$, the PAPR constraint becomes the constant-modulus constraint, i.e., the constraint in (12) can be expressed as

$$|s(l)| = a_s, l = 1, \dots, L, \quad (14)$$

where $a_s = \sqrt{e_t/L}$. If $\rho = L$, the constraint $\text{PAPR}(\mathbf{s}) \leq \rho$ is redundant and the PAPR constraint becomes the energy constraint.

- Spectral constraint. The increasing demand of a larger bandwidth for radar and communication systems results in a crowded spectrum and mutual interference [29], [39], [41]–[44]. To improve the performance and reduce the interference for a radar operating in spectrally crowded environments, we enforce a spectral constraint on the waveform (see a similar constraint in [39], [43], [45], [46]):

$$\mathbf{s}^\dagger \mathbf{s} = e_t, \mathbf{s}^\dagger \mathbf{R}_I \mathbf{s} \leq E_I, \quad (15)$$

where E_I is the maximum allowed interference that can be tolerated by the communication systems, $\mathbf{R}_I = \sum_{k=1}^{K_{\text{rad}}} w_k \mathbf{R}_{I,k}$, K_{rad} is the number of nearby communication systems, w_k is the weight corresponding to the k th communication system (which is a user-defined parameter and represents different emphasis on various communication systems),

$$\mathbf{R}_{I,k}(m, n) = \begin{cases} f_2^k - f_1^k, & m = n \\ \frac{e^{j2\pi f_2^k(m-n)} - e^{j2\pi f_1^k(m-n)}}{j2\pi(m-n)} & m \neq n, \end{cases}$$

f_2^k and f_1^k are the upper and the lower normalized frequencies of the k th communication system, respectively. Note that f_2^k and f_1^k can be obtained from spectral regulations, or by spectrum sensing (e.g., by a cognitive radar [29], [43]).

III. MINORIZER CONSTRUCTION

Note that the optimization problems in (6) and (9) are in general non-convex. To tackle the non-convex optimization problems, we develop a unified optimization framework in this section. Specifically, the framework is based on MM (see, e.g., [47], [48] for a tutorial introduction to the MM algorithms). The key idea of the proposed framework is to derive minorizers for $f_I(\mathbf{s})$ and $f_E(\mathbf{s})$. In precise, the derived minorizers (denoted by $g_O(\mathbf{s}; \mathbf{s}_k)$) should satisfy that

$$g_O(\mathbf{s}; \mathbf{s}_k) \leq f_O(\mathbf{s}), \quad (16a)$$

$$g_O(\mathbf{s}_k; \mathbf{s}_k) = f_O(\mathbf{s}_k), \quad (16b)$$

where $O = I$ or E .

A. Minorizer for $f_I(\mathbf{s})$

Note that the objective function in (6) can be rewritten as

$$f_I(\mathbf{s}) = \log \det(\mathbf{R}_h^{\frac{1}{2}} \mathbf{S}^\dagger \mathbf{R}_n^{-1} \mathbf{S} \mathbf{R}_h^{\frac{1}{2}} + \mathbf{I}), \quad (17)$$

where we have used the fact that $\det(\mathbf{I} + \mathbf{A}\mathbf{B}) = \det(\mathbf{I} + \mathbf{B}\mathbf{A})$ [33]. Using the matrix inversion lemma yields [33]

$$\begin{aligned} (\mathbf{R}_h^{\frac{1}{2}} \mathbf{S}^\dagger \mathbf{R}_n^{-1} \mathbf{S} \mathbf{R}_h^{\frac{1}{2}} + \mathbf{I})^{-1} &= \mathbf{I} - \mathbf{R}_h^{\frac{1}{2}} \mathbf{S}^\dagger \mathbf{R}_s^{-1} \mathbf{S} \mathbf{R}_h^{\frac{1}{2}} \\ &= (\mathbf{K}\mathbf{M}^{-1}\mathbf{K}^\dagger)^{-1}, \end{aligned} \quad (18)$$

where $\mathbf{K} = [\mathbf{I}_P, \mathbf{0}_{P \times L_0}]$, and

$$\mathbf{M} = \begin{bmatrix} \mathbf{I} & \mathbf{R}_h^{\frac{1}{2}} \mathbf{S}^\dagger \\ \mathbf{S} \mathbf{R}_h^{\frac{1}{2}} & \mathbf{R}_s \end{bmatrix}. \quad (19)$$

Thus, we have

$$f_I(\mathbf{s}) = \log \det(\mathbf{K}\mathbf{M}^{-1}\mathbf{K}^\dagger). \quad (20)$$

It follows from Lemma 1 of [49] that $\log \det(\mathbf{K}\mathbf{M}^{-1}\mathbf{K}^\dagger)$ is a convex function of \mathbf{M} . Since convex functions are minorized by their supporting hyperplanes [50], we have

$$\log \det(\mathbf{K}\mathbf{M}^{-1}\mathbf{K}^\dagger) \geq \log \det(\mathbf{K}\mathbf{M}_k^{-1}\mathbf{K}^\dagger) + \text{tr}(\mathbf{G}_k(\mathbf{M} - \mathbf{M}_k)),$$

where

$$\mathbf{G}_k = -\mathbf{M}_k^{-1}\mathbf{K}^\dagger(\mathbf{K}\mathbf{M}_k^{-1}\mathbf{K}^\dagger)^{-1}\mathbf{K}\mathbf{M}_k^{-1} \quad (21)$$

is the gradient of $\log \det(\mathbf{K}\mathbf{M}^{-1}\mathbf{K}^\dagger)$ at \mathbf{M}_k (which can be verified by using the results from [51]),

$$\mathbf{M}_k = \begin{bmatrix} \mathbf{I} & \mathbf{R}_h^{\frac{1}{2}} \mathbf{S}_k^\dagger \\ \mathbf{S}_k \mathbf{R}_h^{\frac{1}{2}} & \mathbf{R}_{s,k} \end{bmatrix}, \quad (22)$$

$\mathbf{R}_{s,k} = \mathbf{S}_k \mathbf{R}_h \mathbf{S}_k^\dagger + \mathbf{R}_n$, and \mathbf{S}_k is formed by $\mathbf{s}_k \in \mathcal{S}$ (which is the waveform at the k th iteration).

Let us partition \mathbf{G}_k as

$$\mathbf{G}_k = \begin{bmatrix} \mathbf{G}_k^{11} & \mathbf{G}_k^{12} \\ \mathbf{G}_k^{21} & \mathbf{G}_k^{22} \end{bmatrix}, \quad (23)$$

where $\mathbf{G}_k^{11} \in \mathbb{C}^{P \times P}$, $\mathbf{G}_k^{12} = (\mathbf{G}_k^{21})^\dagger \in \mathbb{C}^{P \times L_0}$, and $\mathbf{G}_k^{22} \in \mathbb{C}^{L_0 \times L_0}$. Define $\mathbf{L} = [\mathbf{0}_{L_0 \times P}, \mathbf{I}_{L_0}]$. Then we have

$$\mathbf{G}_k^{11} = \mathbf{K}\mathbf{G}_k\mathbf{K}^\dagger = -(\mathbf{R}_h^{\frac{1}{2}} \mathbf{S}_k^\dagger \mathbf{R}_n^{-1} \mathbf{S}_k \mathbf{R}_h^{\frac{1}{2}} + \mathbf{I}), \quad (24)$$

$$\mathbf{G}_k^{21} = \mathbf{L}\mathbf{G}_k\mathbf{K}^\dagger = -\mathbf{R}_n^{-1} \mathbf{S}_k \mathbf{R}_h^{\frac{1}{2}}, \quad (25)$$

$$\mathbf{G}_k^{22} = \mathbf{L}\mathbf{G}_k\mathbf{L}^\dagger = -\mathbf{G}_k^{21}(\mathbf{K}\mathbf{M}_k^{-1}\mathbf{K}^\dagger)^{-1}\mathbf{G}_k^{12}. \quad (26)$$

Using the matrix inversion lemma and after some algebraic manipulations, \mathbf{G}_k^{22} can be simplified into

$$\mathbf{G}_k^{22} = \mathbf{R}_{s,k}^{-1} - \mathbf{R}_n^{-1}. \quad (27)$$

Using the partition of \mathbf{G}_k in (23), we have

$$\begin{aligned} \text{tr}(\mathbf{G}_k \mathbf{M}) &= \text{tr}(\mathbf{G}_k^{11}) + \text{tr}(\mathbf{G}_k^{22} \mathbf{R}_n) + 2\text{Re}(\text{tr}(\mathbf{S}_k^\dagger \mathbf{G}_k^{21} \mathbf{R}_h^{\frac{1}{2}})) \\ &\quad + \text{tr}(\mathbf{G}_k^{22} \mathbf{S} \mathbf{R}_h \mathbf{S}^\dagger). \end{aligned} \quad (28)$$

Thus, $f_1(\mathbf{s})$ is minorized by

$$g_1(\mathbf{s}; \mathbf{s}_k) = c_1 + 2\text{Re}(\text{tr}(\mathbf{S} \mathbf{R}_h^{\frac{1}{2}} \mathbf{G}_k^{12})) + \text{tr}(\mathbf{G}_k^{22} \mathbf{S} \mathbf{R}_h \mathbf{S}^\dagger), \quad (29)$$

where $c_1 = \text{tr}(\mathbf{G}_k^{11}) + \text{tr}(\mathbf{G}_k^{22} \mathbf{R}_n) + \log \det(\mathbf{K}\mathbf{M}_k^{-1}\mathbf{K}^\dagger) - \text{tr}(\mathbf{G}_k \mathbf{M}_k)$.

Proposition 1: Define $\mathbf{E} = [\mathbf{E}_1^T, \mathbf{E}_2^T, \dots, \mathbf{E}_P^T]^T$, $\mathbf{E}_p = [\mathbf{0}_{L \times (p-1)}, \mathbf{I}_L, \mathbf{0}_{L \times (P-p)}]^T \in \mathbb{C}^{L_0 \times L}$, $p = 1, \dots, P$, then we have

$$g_1(\mathbf{s}; \mathbf{s}_k) = c_1 + 2\text{Re}(\mathbf{s}^\dagger \mathbf{a}_{\mathbf{I},k}) + \mathbf{s}^\dagger \mathbf{A}_{\mathbf{I},k} \mathbf{s}, \quad (30)$$

where $\mathbf{a}_{\mathbf{I},k} = \mathbf{E}^\dagger \text{vec}(\mathbf{G}_k^{21} \mathbf{R}_h^{\frac{1}{2}})$, $\mathbf{A}_{\mathbf{I},k} = \mathbf{E}^\dagger (\mathbf{R}_h^* \otimes \mathbf{G}_k^{22}) \mathbf{E}$.

Proof: See Appendix B. ■

According to Proposition 1, the mutual information maximization problem of an MM algorithm based on (29) (at the $(k+1)$ th iteration) can be reformulated as

$$\begin{aligned} \max_{\mathbf{s}} g_1(\mathbf{s}; \mathbf{s}_k) &= c_1 + 2\text{Re}(\mathbf{s}^\dagger \mathbf{a}_{\mathbf{I},k}) + \mathbf{s}^\dagger \mathbf{A}_{\mathbf{I},k} \mathbf{s} \\ \text{s.t. } \mathbf{s} &\in \mathcal{S}. \end{aligned} \quad (31)$$

B. Minorizer for $f_E(\mathbf{s})$

Lemma 1: Assume that $\mathbf{B} \succ \mathbf{0}$. Then $\psi(\mathbf{A}, \mathbf{B}) = \text{tr}(\mathbf{A}^\dagger \mathbf{B}^{-1} \mathbf{A})$ is jointly convex w.r.t. \mathbf{A} and \mathbf{B} , and is minorized by

$$\text{tr}(\mathbf{A}^\dagger \mathbf{B}^{-1} \mathbf{A}) \geq 2\text{Re}(\text{tr}(\mathbf{A}_k^\dagger \mathbf{B}_k^{-1} \mathbf{A})) - \text{tr}(\mathbf{B}_k^{-1} \mathbf{A}_k \mathbf{A}_k^\dagger \mathbf{B}_k^{-1} \mathbf{B}). \quad (32)$$

Proof: See Appendix C. ■

Note that $\mathbf{S} \mathbf{R}_h \mathbf{S}^\dagger + \mathbf{R}_n \succ \mathbf{0}$. Using Lemma 1 (by substituting \mathbf{A} with $\mathbf{S} \mathbf{R}_h$ and \mathbf{B} with $\mathbf{S} \mathbf{R}_h \mathbf{S}^\dagger + \mathbf{R}_n$), we obtain

$$\text{tr}(\mathbf{R}_h \mathbf{S}^\dagger (\mathbf{S} \mathbf{R}_h \mathbf{S}^\dagger + \mathbf{R}_n)^{-1} \mathbf{S} \mathbf{R}_h) \geq 2\text{Re}(\text{tr}(\mathbf{H}_k^\dagger \mathbf{S})) - \text{tr}(\mathbf{T}_k (\mathbf{S} \mathbf{R}_h \mathbf{S}^\dagger + \mathbf{R}_n)),$$

where $\mathbf{H}_k = \mathbf{R}_{s,k}^{-1} \mathbf{S}_k \mathbf{R}_h^2$, and $\mathbf{T}_k = \mathbf{R}_{s,k}^{-1} \mathbf{S}_k \mathbf{R}_h^2 \mathbf{S}_k^\dagger \mathbf{R}_{s,k}^{-1}$. Therefore, $f_E(\mathbf{s})$ is minorized by

$$g_E(\mathbf{s}; \mathbf{s}_k) = c_E + 2\text{Re}(\text{tr}(\mathbf{H}_k \mathbf{S})) - \text{tr}(\mathbf{T}_k \mathbf{S} \mathbf{R}_h \mathbf{S}^\dagger), \quad (33)$$

where $c_E = -\text{tr}(\mathbf{T}_k \mathbf{R}_n)$. Similar to that in Proposition 1, $g_E(\mathbf{s}; \mathbf{s}_k)$ can be rewritten as

$$g_E(\mathbf{s}; \mathbf{s}_k) = c_E + 2\text{Re}(\mathbf{s}^\dagger \mathbf{a}_{E,k}) + \mathbf{s}^\dagger \mathbf{A}_{E,k} \mathbf{s}, \quad (34)$$

where $\mathbf{a}_{E,k} = \mathbf{E}^\dagger \text{vec}(\mathbf{H}_k)$, and $\mathbf{A}_{E,k} = -\mathbf{E}^\dagger (\mathbf{R}_h^* \otimes \mathbf{T}_k) \mathbf{E}$.

Therefore, the MMSE minimization problem of an MM algorithm based on (34) (at the $(k+1)$ th iteration) is equivalent to

$$\begin{aligned} \max_{\mathbf{s}} g_E(\mathbf{s}; \mathbf{s}_k) &= c_E + 2\text{Re}(\mathbf{s}^\dagger \mathbf{a}_{E,k}) + \mathbf{s}^\dagger \mathbf{A}_{E,k} \mathbf{s} \\ \text{s.t. } \mathbf{s} &\in \mathcal{S}. \end{aligned} \quad (35)$$

IV. SOLVING THE QUADRATIC PROGRAMMING PROBLEM

In this section, we propose algorithms to solve the following minorized problem (which is a constrained quadratic programming problem) at the $(k+1)$ th iteration:

$$\begin{aligned} \max_{\mathbf{s}} g_O(\mathbf{s}; \mathbf{s}_k) &= c_O + 2\text{Re}(\mathbf{s}^\dagger \mathbf{a}_{O,k}) + \mathbf{s}^\dagger \mathbf{A}_{O,k} \mathbf{s} \\ \text{s.t. } \mathbf{s} &\in \mathcal{S}, \end{aligned} \quad (36)$$

where $\mathbf{O} = \mathbf{I}$ or $\mathbf{O} = \mathbf{E}$.

A. Energy Constraint

The minorized problem under the energy constraint can be formulated as follows:

$$\begin{aligned} \max_{\mathbf{s}} \quad & 2\text{Re}(\mathbf{s}^\dagger \mathbf{a}_{O,k}) + \mathbf{s}^\dagger \mathbf{A}_{O,k} \mathbf{s} \\ \text{s.t.} \quad & \mathbf{s}^\dagger \mathbf{s} \leq e_t. \end{aligned} \quad (37)$$

Note that $\mathbf{A}_{O,k} \preceq \mathbf{0}$ (We refer to Appendix D for the proof). Thus, the optimization problem in (37) is convex, meaning that its globally optimal solution can be found with polynomial time (e.g., via interior point method). In addition, we can derive a semi-closed-form expression of the optimal solution by using the method of Lagrange multipliers. To this end, let the Lagrangian associated with (37) be

$$F(\mathbf{s}, \mu) = -\mathbf{s}^\dagger \mathbf{A}_{O,k} \mathbf{s} - 2\text{Re}(\mathbf{s}^\dagger \mathbf{a}_{O,k}) + \mu(\mathbf{s}^\dagger \mathbf{s} - e_t), \quad (38)$$

where $\mu \geq 0$ is the Lagrange multiplier associated with the energy constraint. According to the Karush-Kuhn-Tucker (KKT) conditions [50], the optimal solution of (37) satisfies

$$\begin{aligned} (\mu_k \mathbf{I} - \mathbf{A}_{O,k}) \mathbf{s} &= \mathbf{a}_{O,k}, \\ \mu_k (\mathbf{s}^\dagger \mathbf{s} - e_t) &= 0. \end{aligned} \quad (39)$$

if $\mu_k \neq 0$, then

$$\mathbf{s} = (\mu_k \mathbf{I} - \mathbf{A}_{O,k})^{-1} \mathbf{a}_{O,k}, \quad (40)$$

where μ_k can be obtained by solving $\mathbf{a}_{O,k}^\dagger (\mu_k \mathbf{I} - \mathbf{A}_{O,k})^{-2} \mathbf{a}_{O,k} = e_t$. Otherwise, the optimal solution is given by $\mathbf{s} = -\mathbf{A}_{O,k}^{-1} \mathbf{a}_{O,k}$.

B. PAPR Constraint

The minorized problem under the PAPR constraint is equivalent to

$$\begin{aligned} \max_{\mathbf{s}} \quad & 2\text{Re}(\mathbf{s}^\dagger \mathbf{a}_{O,k}) + \mathbf{s}^\dagger \mathbf{A}_{O,k} \mathbf{s} \\ \text{s.t.} \quad & \mathbf{s}^\dagger \mathbf{s} = e_t, \text{PAPR}(\mathbf{s}) \leq \rho. \end{aligned} \quad (41)$$

We can also tackle the problem in (41) by MM. To this end, we note that

$$\mathbf{s}^\dagger \mathbf{A}_{O,k} \mathbf{s} \geq 2\text{Re}(\mathbf{s}^\dagger \mathbf{A}_{\text{pos},k} \mathbf{s}_j) + \text{const}_j, \quad (42)$$

where $\mathbf{A}_{\text{pos},k} = \mathbf{A}_{O,k} - \lambda_{\min}(\mathbf{A}_{O,k}) \mathbf{I}$, $\lambda_{\min}(\mathbf{A}_{O,k})$ is the smallest eigenvalue of $\mathbf{A}_{O,k}$, $\text{const}_j = 2\lambda_{\min}(\mathbf{A}_{O,k})e_t - \mathbf{s}_j^\dagger \mathbf{A}_{O,k} \mathbf{s}_j$, and \mathbf{s}_j is the solution at the j th (inner) iteration. As a result, the objective function in (41) is minorized by

$$2\text{Re}(\mathbf{s}^\dagger \mathbf{t}_{k,j}) + \text{const}_j, \quad (43)$$

where $\mathbf{t}_{k,j} = \mathbf{a}_{O,k} + \mathbf{A}_{\text{pos},k}\mathbf{s}_j$. Thus, the maximization problem of an MM algorithm based on (43) is

$$\begin{aligned} \max_{\mathbf{s}} \quad & 2\text{Re}(\mathbf{s}^\dagger \mathbf{t}_{k,j}) \\ \text{s.t.} \quad & \mathbf{s}^\dagger \mathbf{s} = e_t, \text{PAPR}(\mathbf{s}) \leq \rho. \end{aligned} \quad (44)$$

The above optimization problem can be solved by Algorithm 2 in [52]. In particular, if $\rho = 1$, a closed-form expression for the optimal solution can be derived as

$$s_l = a_s \exp(j\phi_{t,l}), \quad (45)$$

where $\phi_{t,l} = \arg(t_l)$, and t_l is the l th element of $\mathbf{t}_{k,j}$.

Algorithm 1 summarizes the procedure to tackle the PAPR-constrained optimization problem in (41).

Algorithm 1: Optimization algorithm for (41).

Input: $\mathbf{A}_{O,k}$, $\mathbf{a}_{O,k}$, $\lambda_{\min}(\mathbf{A}_{O,k})$, ρ .

Output: \mathbf{s}_{k+1} .

1 **Initialize:** $j = 0$, $\mathbf{s}_{k,j} = \mathbf{s}_k$, $\mathbf{A}_{\text{pos},k} = \mathbf{A}_{O,k} - \lambda_{\min}(\mathbf{A}_{O,k})\mathbf{I}$.

2 **repeat**

3 $\mathbf{t}_{k,j} = \mathbf{a}_{O,k} + \mathbf{A}_{\text{pos},k}\mathbf{s}_j$
 4 Update $\mathbf{s}_{k,j+1}$ by solving the optimization problem in (44)
 5 $j = j + 1$

6 **until** convergence;

7 $\mathbf{s}_{k+1} = \mathbf{s}_{k,j}$

C. Spectral Constraint

The minorized problem under the spectral constraint is given by

$$\begin{aligned} \max_{\mathbf{s}} \quad & 2\text{Re}(\mathbf{s}^\dagger \mathbf{a}_{O,k}) + \mathbf{s}^\dagger \mathbf{A}_{O,k} \mathbf{s} \\ \text{s.t.} \quad & \mathbf{s}^\dagger \mathbf{s} = e_t, \mathbf{s}^\dagger \mathbf{R}_1 \mathbf{s} \leq E_1. \end{aligned} \quad (46)$$

The optimization problem in (46) is hidden-convex. Thus, it can be solved by semi-definite relaxation followed by a rank-one decomposition [53]. However, the computational complexity of solving a semi-definite programming problem is high ($O(L^{4.5})$, given that the primal-dual path following method is used). We propose using the alternating direction method of multipliers (ADMM) [54] to reduce the computational complexity (As shown in Table I, the proposed ADMM has a complexity of $O(L^3)$). To

apply the ADMM algorithm to this problem, we use the variable splitting trick and introduce an auxiliary variable \mathbf{u} as follows:

$$\begin{aligned} \min_{\mathbf{s}, \mathbf{u}} \quad & 2\text{Re}(\mathbf{s}^\dagger \bar{\mathbf{a}}_{O,k}) + \mathbf{s}^\dagger \bar{\mathbf{A}}_{O,k} \mathbf{s} \\ \text{s.t.} \quad & \mathbf{s}^\dagger \mathbf{s} = e_t, \mathbf{u}^\dagger \mathbf{R}_I \mathbf{u} \leq E_I, \mathbf{s} = \mathbf{u}, \end{aligned} \quad (47)$$

where $\bar{\mathbf{A}}_{O,k} = -\mathbf{A}_{O,k}$, and $\bar{\mathbf{a}}_{O,k} = -\mathbf{a}_{O,k}$. The augmented Lagrangian associated with the optimization problem in (47) can be written as

$$\begin{aligned} L_\varrho(\mathbf{s}, \mathbf{u}, \boldsymbol{\lambda}) = & \mathbf{s}^\dagger \bar{\mathbf{A}}_{O,k} \mathbf{s} + 2\text{Re}(\mathbf{s}^\dagger \bar{\mathbf{a}}_{O,k}) + 2\text{Re}(\boldsymbol{\lambda}^\dagger (\mathbf{s} - \mathbf{u})) \\ & + \varrho \|\mathbf{s} - \mathbf{u}\|_2^2, \end{aligned} \quad (48)$$

where $\boldsymbol{\lambda}$ is the Lagrange multiplier, and ϱ is the penalty parameter. The ADMM method consists of the following iterations:

$$\mathbf{s}_{j+1} = \arg \min_{\mathbf{s}} L_\varrho(\mathbf{s}, \mathbf{u}_j, \boldsymbol{\lambda}_j), \quad (49a)$$

$$\mathbf{u}_{j+1} = \arg \min_{\mathbf{u}} L_\varrho(\mathbf{s}_{j+1}, \mathbf{u}, \boldsymbol{\lambda}_j), \quad (49b)$$

$$\boldsymbol{\lambda}_{j+1} = \boldsymbol{\lambda}_j + \varrho(\mathbf{s} - \mathbf{u}). \quad (49c)$$

The optimization problem in (49a) can be rewritten as

$$\begin{aligned} \min_{\mathbf{s}} \quad & \mathbf{s}^\dagger (\bar{\mathbf{A}}_{O,k} + \varrho \mathbf{I}) \mathbf{s} + 2\text{Re}(\mathbf{s}^\dagger \mathbf{b}_{O,k}) \\ \text{s.t.} \quad & \mathbf{s}^\dagger \mathbf{s} = e_t, \end{aligned} \quad (50)$$

where $\mathbf{b}_{O,k} = \bar{\mathbf{a}}_{O,k} + \boldsymbol{\lambda}_j - \varrho \mathbf{u}_j$. The optimal solution of (50) can be obtained similarly to that in (37):

$$\mathbf{s}_{j+1} = (\bar{\mathbf{A}}_{O,k} + (\varrho + \alpha_1) \mathbf{I})^{-1} \mathbf{b}_{O,k}, \quad (51)$$

where α_1 is a scalar making $\mathbf{s}_{j+1}^\dagger \mathbf{s}_{j+1} = e_t$.

The optimization problem in (49b) is equivalent to

$$\begin{aligned} \min_{\mathbf{u}} \quad & \|\mathbf{u} - \mathbf{d}_j\|_2^2 \\ \text{s.t.} \quad & \mathbf{u}^\dagger \mathbf{R}_I \mathbf{u} \leq E_I, \end{aligned} \quad (52)$$

where $\mathbf{d}_j = \mathbf{s}_{j+1} + \boldsymbol{\lambda}_j / \varrho$. Its solution is given by (see [55] for more details):

$$\mathbf{u}_{j+1} = \begin{cases} \mathbf{d}_j, & \text{if } \mathbf{d}_j^\dagger \mathbf{R}_I \mathbf{d}_j \leq E_I, \\ (\mathbf{I} + \alpha_2 \mathbf{R}_I)^{-1} \mathbf{d}_j, & \text{if } \mathbf{d}_j^\dagger \mathbf{R}_I \mathbf{d}_j > E_I, \end{cases} \quad (53)$$

where α_2 can be obtained by solving $\mathbf{d}_j^\dagger \mathbf{T}_I \mathbf{d}_j = E_I$, and $\mathbf{T}_I = (\mathbf{I} + \alpha_2 \mathbf{R}_I)^{-1} \mathbf{R}_I (\mathbf{I} + \alpha_2 \mathbf{R}_I)^{-1}$.

Algorithm 2 summarizes the proposed ADMM algorithm for (46), where we terminate the ADMM algorithm if both the (Euclidian) norm of the primal residual \mathbf{r}_j and the dual residual \mathbf{d}_j are sufficiently small, where $\mathbf{r}_j = \mathbf{s}_j - \mathbf{u}_j$, and $\mathbf{d}_j = \varrho(\mathbf{s}_j - \mathbf{s}_{j+1})$.

Algorithm 2: Optimization algorithm for (46).

Input: $\mathbf{A}_{O,k}, \mathbf{a}_{O,k}, e_t, E_1$.

Output: \mathbf{s}_{k+1} .

1 **Initialize:** $\varrho, \mathbf{u} = \mathbf{0}, \boldsymbol{\lambda} = \mathbf{0}, j = 0, \mathbf{s}_{k,j} = \mathbf{s}_k$.

2 **repeat**

3 Update $\mathbf{s}_{k,j+1}$ by (51)

4 $\mathbf{d}_{k,j} = \mathbf{s}_{k,j+1} + \boldsymbol{\lambda}_j / \varrho$

5 Update $\mathbf{u}_{k,j+1}$ by (53)

6 $\boldsymbol{\lambda}_{j+1} = \boldsymbol{\lambda}_j + \varrho(\mathbf{s}_{k,j+1} - \mathbf{u}_{k,j+1})$

7 $j = j + 1$

8 **until** *convergence*;

9 $\mathbf{s}_{k+1} = \mathbf{s}_{k,j}$

V. ALGORITHM SUMMARY AND SOME DISCUSSIONS

A. Algorithm Summary and Convergence

We summarize the proposed algorithm framework in Algorithm 3. Note that in some applications, to control the shape of the ambiguity function or achieve some desired property, one needs to enforce a similarity constraint on the waveform [56], which can be written as

$$\mathbf{s}^\dagger \mathbf{s} = e_t, \|\mathbf{s} - \mathbf{s}_0\|_2^2 \leq \varepsilon_2, \quad (54)$$

where \mathbf{s}_0 denotes a reference waveform possessing certain desirable property, $\mathbf{s}_0^\dagger \mathbf{s}_0 = e_t$, and ε_2 is a user specified similarity parameter ($0 \leq \varepsilon_2 \leq 2e_t$). One can also enforce both constant-modulus and similarity constraints on the waveform [34], [39]. The associated constraints are given by

$$|s_l| = a_s, l = 1, \dots, L, \|\mathbf{s} - \mathbf{s}_0\|_\infty \leq \varepsilon_\infty, \quad (55)$$

where the reference waveform \mathbf{s}_0 is constant-modulus, and ε_∞ denotes a similarity parameter ($0 \leq \varepsilon_\infty \leq 2a_s$). It can be verified that the proposed framework can be applied to deal with both the constraints in (54) and (55). Nevertheless, we omit the details here due to space limitations.

Algorithm 3: Waveform optimization algorithm for radar range profiling.

Input: $\mathbf{R}_h, \mathbf{R}_n$.

Output: \mathbf{s} .

```

1 Initialize:  $k = 0, \mathbf{s}_k$ .
2 repeat
3   switch Design metric do
4     case Maximizing mutual information do
5       Compute  $\mathbf{G}_k^{22}$  using (27) and  $\mathbf{G}_k^{21}$  using (25)
6       Compute  $\mathbf{A}_{I,k}$  and  $\mathbf{a}_{I,k}$ 
7        $\mathbf{A}_{O,k} = \mathbf{A}_{I,k}, \mathbf{a}_{O,k} = \mathbf{a}_{I,k}$ 
8     case Minimizing MMSE do
9       Compute  $\mathbf{H}_k$  and  $\mathbf{T}_k$ 
10      Compute  $\mathbf{A}_{E,k}$  and  $\mathbf{a}_{E,k}$ 
11       $\mathbf{A}_{O,k} = \mathbf{A}_{E,k}, \mathbf{a}_{O,k} = \mathbf{a}_{E,k}$ 
12    end
13  end
14  switch Constraint do
15    case Energy constraint do
16      Update  $\mathbf{s}_{k+1}$  by (40)
17    case PAPR constraint do
18      Update  $\mathbf{s}_{k+1}$  by Algorithm 1
19    case Spectral constraint do
20      Update  $\mathbf{s}_{k+1}$  by Algorithm 2
21    end
22  end
23   $k = k + 1$ 
24 until convergence;

```

TABLE I
COMPUTATIONAL COMPLEXITY ANALYSIS

Computation	Complexity	Computation	Complexity
<i>Mutual information maximization</i>		<i>MMSE minimization</i>	
\mathbf{G}_k^{22}	$O(L_0^3)$	\mathbf{H}_k	$O(L_0^3 + L_0^2P + L_0P^2)$
\mathbf{G}_k^{21}	$O(L_0^2P + L_0P^2)$	\mathbf{T}_k	$O(L_0^2P^2)$
$\mathbf{A}_{I,k}$	$O(L_0^2P^2)$	$\mathbf{A}_{E,k}$	$O(L_0^2P^2)$
$\mathbf{a}_{I,k}$	$O(L_0^2P^2)$	$\mathbf{a}_{E,k}$	-
<i>Solving the quadratic programming problem</i>			
Energy constraint	$O(L^3)$		
PAPR constraint	$O(N_{papr}L^2)$		
Spectral constraint	$O(N_{spectral}L^3)$		

Next we analyze the convergence of the proposed algorithm. Note that $f_O(\mathbf{s}_{k+1}) \geq g_O(\mathbf{s}_{k+1}; \mathbf{s}_k)$ and $f_O(\mathbf{s}_k) = g_O(\mathbf{s}_k; \mathbf{s}_k)$. Thus, if $g_O(\mathbf{s}_{k+1}; \mathbf{s}_k) \geq g_O(\mathbf{s}_k; \mathbf{s}_k)$, then $f_O(\mathbf{s}_{k+1}) \geq f_O(\mathbf{s}_k)$, and the convergence of the sequence of the objective values is guaranteed. For the energy constraint, $g_O(\mathbf{s}_{k+1}; \mathbf{s}_k) \geq g_O(\mathbf{s}_k; \mathbf{s}_k)$ owing to the optimality of \mathbf{s}_{k+1} given \mathbf{s}_k ; for the PAPR constraint, if \mathbf{s}_k is used as the starting point of the proposed MM method, the improvement of $g_O(\mathbf{s}_{k+1}; \mathbf{s}_k)$ over $g_O(\mathbf{s}_k; \mathbf{s}_k)$ can be verified by using the ascent property of the MM method; for the spectral constraint, if \mathbf{s}_{k+1} is obtained by the SDR and rank-one decomposition, \mathbf{s}_{k+1} is the optimal solution given \mathbf{s}_k , and it can be checked that $g_O(\mathbf{s}_{k+1}; \mathbf{s}_k) \geq g_O(\mathbf{s}_k; \mathbf{s}_k)$. Otherwise, if \mathbf{s}_{k+1} is obtained by the proposed ADMM method, it is non-trivial to prove the optimality of \mathbf{s}_{k+1} . However, for the proposed ADMM algorithm, we do not encounter any convergence problem during the numerical simulations (possibly because of the hidden convexity of the problem in (46)).

B. Computational Complexity

Table I summarizes the per-iteration computational complexity of the proposed algorithms, where N_{papr} is the number of (inner) iterations needed to reach convergence under the PAPR constraint, and $N_{spectral}$ is the number of (inner) iterations needed to reach convergence under the spectral constraint. Note that we have ignored the computational complexity that can be performed offline (e.g., the calculation of \mathbf{R}_n^{-1}). In addition, we ignore the computational complexity involving the multiplication of \mathbf{E} , since it can be done by addition.

C. Connection with ZCZ Waveforms

Suppose that $\mathbf{R}_n = \sigma_0^2 \mathbf{I}$ (e.g., the disturbance is dominated by the white noise) and $\mathbf{R}_h = \mathbf{\Lambda}_h$ (i.e., the uncertainty of each element of the target impulse response vector is independent). Then the waveform design problem based on maximizing mutual information can be rewritten as

$$\begin{aligned} \max_{\mathbf{s}} f_1(\mathbf{s}) &= \log \det(\sigma_0^{-2} \mathbf{S}^\dagger \mathbf{S} + \mathbf{\Lambda}_h^{-1}) \\ \text{s.t. } \mathbf{s} &\in \mathcal{S}. \end{aligned} \quad (56)$$

Note that

$$\mathbf{S}^\dagger \mathbf{S} = e_t \begin{pmatrix} 1 & r_1^* & \cdots & r_{P-1}^* \\ r_1 & 1 & \cdots & r_{P-2}^* \\ \vdots & \vdots & \ddots & \vdots \\ r_{P-1} & r_{P-2} & \cdots & 1 \end{pmatrix}, \quad (57)$$

where $r_p = \frac{1}{e_t} \sum_{k=1}^{L-p} s_k^* s_{k+p}$ is the aperiodic correlation function of \mathbf{s} . In addition, according to Hadamard's inequality [33],

$$\det(\sigma_0^{-2} \mathbf{S}^\dagger \mathbf{S} + \mathbf{\Lambda}_h^{-1}) \leq \prod_{p=1}^P (\sigma_0^{-2} e_t + \lambda_{h,p}^{-1}), \quad (58)$$

where $\lambda_{h,p}$ is the p th diagonal element of $\mathbf{\Lambda}_h$, and the equality holds if and only if $\mathbf{S}^\dagger \mathbf{S}$ is diagonal. Thus, to maximize the mutual information, the correlation function of \mathbf{s} should satisfy that $r_p \approx 0, p = 1, \dots, P-1$. The corresponding waveform is called zero-correlation zone (ZCZ) waveform [57].

Under the same assumption, the waveform design problem based on minimizing MMSE can be reformulated by

$$\begin{aligned} \min_{\mathbf{s}} \text{tr} \left(\left[\mathbf{\Lambda}_h^{-1} + \sigma_0^{-2} \mathbf{S}^\dagger \mathbf{S} \right]^{-1} \right) \\ \text{s.t. } \mathbf{s} \in \mathcal{S}. \end{aligned} \quad (59)$$

Note that [58]

$$\text{tr} \left(\left[\mathbf{\Lambda}_h^{-1} + \sigma_0^{-2} \mathbf{S}^\dagger \mathbf{S} \right]^{-1} \right) \geq \sum_{p=1}^P \frac{1}{\lambda_{h,p}^{-1} + \sigma_0^{-2} e_t}, \quad (60)$$

where the equality holds if and only if $\mathbf{S}^\dagger \mathbf{S}$ is diagonal. Thus, in this situation, the ZCZ waveform also minimizes the MMSE.

D. Mutual Information, MMSE, and SNR

If $P = 1$ (i.e., a point-like target), the mutual information in (5) can be written as

$$\begin{aligned} \log \det(\mathbf{R}_n^{-1} \mathbf{S} \mathbf{R}_h \mathbf{S}^\dagger + \mathbf{I}) &= \log(1 + \lambda_h \mathbf{s}^\dagger \mathbf{R}_n^{-1} \mathbf{s}) \\ &= \log(1 + \lambda_h \text{SNR}), \end{aligned} \quad (61)$$

where we define $\text{SNR} = \mathbf{s}^\dagger \mathbf{R}_n^{-1} \mathbf{s}$. On the other hand, note that the MMSE for this case is given by

$$\text{MMSE} = \frac{1}{\lambda_h^{-1} + \mathbf{s}^\dagger \mathbf{R}_n^{-1} \mathbf{s}} = \frac{1}{\lambda_h^{-1} + \text{SNR}}. \quad (62)$$

Thus, the minimization of MMSE, the maximization of mutual information, and the maximization of SNR are equivalent for the case of $P = 1$.

For the more general case that $P > 1$ and $\boldsymbol{\mu}_h = \mathbf{0}$, if $\lambda_{\max}(\mathbf{R}_n^{-1} \mathbf{S} \mathbf{R}_h \mathbf{S}^\dagger) \ll 1$ (corresponding to the case that SNR is low), where $\lambda_{\max}(\mathbf{R}_n^{-1} \mathbf{S} \mathbf{R}_h \mathbf{S}^\dagger)$ is the largest eigenvalue of $\mathbf{R}_n^{-1} \mathbf{S} \mathbf{R}_h \mathbf{S}^\dagger$, the mutual information in (5) can be approximated by

$$\begin{aligned} \log \det(\mathbf{R}_n^{-1} \mathbf{S} \mathbf{R}_h \mathbf{S}^\dagger + \mathbf{I}) &\approx \text{tr}(\mathbf{R}_n^{-1} \mathbf{S} \mathbf{R}_h \mathbf{S}^\dagger) \\ &= \mathbf{s}^\dagger \mathbf{E}^\dagger (\mathbf{R}_h^* \otimes \mathbf{R}_n^{-1}) \mathbf{E} \mathbf{s}. \end{aligned} \quad (63)$$

By using the low SNR assumption, it can be checked that we can obtain the globally optimal solutions to both the energy-constrained and the spectrally constrained waveform design problems.

VI. NUMERICAL EXAMPLES

In this section, we provide several numerical examples to demonstrate the performance of the proposed algorithms. Unless otherwise stated, the code length of the waveform is $L = 100$. The target occupies $P = 10$ range bins. The mean of the target impulse response is $\boldsymbol{\mu}_h = [5, 5, \dots, 5]^T$ and the covariance matrix is \mathbf{I}_P . We model the disturbance covariance matrix like that in [36], [37]:

$$\mathbf{R}_n = \sigma_J^2 \mathbf{R}_J + \sigma^2 \mathbf{I}, \quad (64)$$

where $\sigma_J^2 = 1000$ and $\sigma^2 = 1$ are the jamming and noise powers, respectively, the (m, n) th element of the jamming covariance matrix \mathbf{R}_J is given by q_{m-n} ($m \geq n$), $[q_0, q_1, \dots, q_{L_0-1}, q_{L_0-1}^*, \dots, q_1^*]^T$ can be obtained by the inverse discrete Fourier transform (IDFT) of $\{\eta_p\}_{p=1}^{2L_0-1}$, and $\{\eta_p\}$ denotes the jamming power spectrum at the frequency $(p-1)/(2L_0-1)$, $p = 1, 2, \dots, 2L_0-1$. For simplicity, we consider a barrage jamming whose power spectrum is given by

$$\eta_p = \begin{cases} 1 & \lfloor (2L_0-1)f_{1,J} \rfloor \leq p \leq \lfloor (2L_0-1)f_{2,J} \rfloor, \\ 0 & \text{otherwise,} \end{cases} \quad (65)$$

where $f_{1,J} = 0.1$, and $f_{1,J} = 0.3$. The available transmit energy is $e_t = L$. We terminate the proposed algorithms if $|f_0(\mathbf{s}_{k+1}) - f_0(\mathbf{s}_k)|/f_0(\mathbf{s}_{k+1}) \leq \varepsilon$, where $\varepsilon = 10^{-4}$. Finally, all the analysis is carried out on a standard laptop with Intel Core i7-8550U and 8 GB RAM.

A. Constant-modulus Constraint

In this subsection, we analyze the performance of the synthesized constant-modulus waveforms. Fig. 2 shows the objective values (including mutual information in Fig. 2(a) and MMSE in Fig. 2(b)) of the waveforms synthesized by the proposed algorithms versus CPU time, where we initialize the proposed algorithms with the LFM waveform (i.e., the k th element of the waveform is given by $\sqrt{e_t/L} \exp(j\pi(k-1)^2/L)$). Moreover, we plot the objective values associated with the energy-constrained waveforms as a benchmark. Note that the curves associated with the objective values (mutual information or MMSE) have monotonically (increasing/decreasing) behaviors. In addition, the objective values of the synthesized constant-modulus waveforms at convergence are close to those of the energy-constrained waveforms. In Fig. 3, we plot the (normalized) energy spectral density (ESD) of the constant-modulus waveforms synthesized by the proposed algorithms. Interestingly, we can observe that the ESDs of the synthesized waveforms form a notch in the frequency band where the barrage jamming exists (shaded in light gray). However, the relationship of the notch depth in this frequency band with the jamming power is unknown.

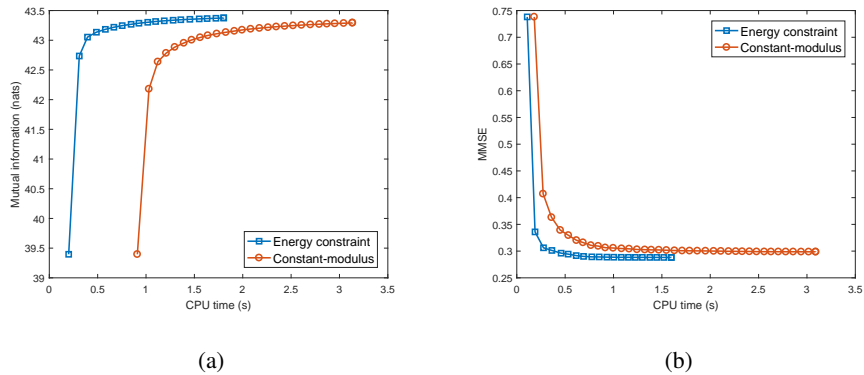


Fig. 2. Convergence of the objective values versus CPU time. PAPR constraint. $\rho = 1$. (a) Mutual information. (b) MMSE.

To analyze the impact of starting points on the performance of the proposed algorithms, we use the same parameters as Fig. 2 and conduct 50 independent Monte Carlo runs using random-phase waveforms as starting points for \mathbf{s} . Specifically, the magnitude of the random-phase waveforms is a_s , and the phases are independent random variables uniformly distributed in $[0, 2\pi]$. Fig. 4 shows the objective values (mutual information or MMSE) at convergence for different starting points, and plots the values of the synthesized

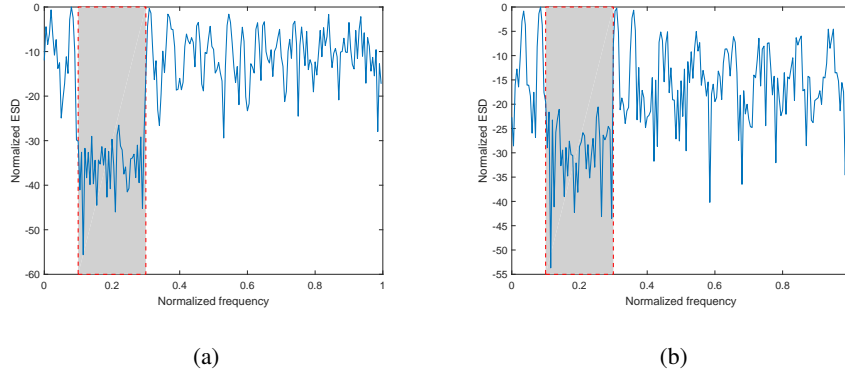


Fig. 3. The ESD of the synthesized constant-modulus waveform at convergence. (a) Mutual information. (b) MMSE.

waveforms in Fig. 2 (which is initialized by LFM). We notice that for all the runs, the objective values at convergence are almost identical to that of the synthesized waveforms in Fig. 2. Therefore, the proposed algorithms are insensitive to the starting points.

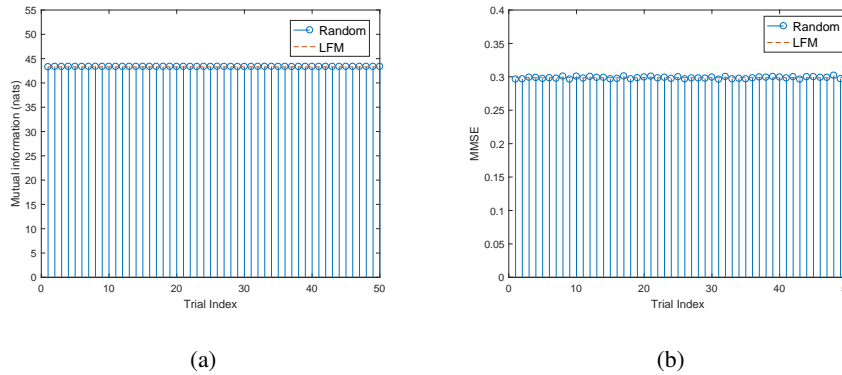


Fig. 4. The impact of starting points on the performance of the synthesized waveforms. (a) Mutual information. (b) MMSE.

Next we compare the performance of the constant-modulus waveforms synthesized by the proposed algorithms with that of the LFM waveform as well as the waveform designed based on maximizing the signal to interference-plus-noise ratio (SINR) (see, e.g., [14], [15], [35], [36] for extensive discussions on this topic). We use a similar method to that in [14] to synthesize the waveform maximizing the SINR. Note that the algorithm in [14] cannot deal with the constant-modulus constraint. To adapt the algorithm in [14] to tackle the constant-modulus waveform design problem, we resort to Algorithm 1 proposed in Section IV-B. Fig. 5 shows the performance of different waveforms versus the code length. For each waveform, the available transmit energy is $e_t = L$ (i.e., the transmit energy is the same for different waveforms but varies with the code length). We can observe that the performance of the waveforms

designed based on maximizing SINR is poor. Note that such waveforms are designed to enhance the detection performance of the radar systems, but not for range profiling. Thus, it is important to adapt the transmit waveform according to the radar tasks. In addition, the waveforms based on maximizing mutual information achieve the largest mutual information and the waveforms based on minimizing the MMSE achieve the smallest MSE. Interestingly, although different criteria are used, the performance of the waveforms designed based on maximizing mutual information is close to that of the waveforms based on minimizing MMSE. Moreover, both kinds of waveforms outperform the conventional LFM waveforms.

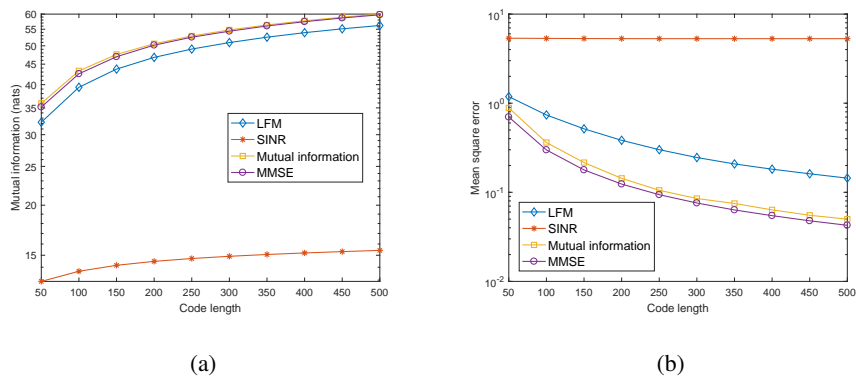


Fig. 5. The performance of the synthesized constant-modulus waveforms versus code length. $e_t = L$. (a) Mutual information. (b) MMSE.

B. Spectral Constraint

In this subsection, we analyze the performance of the spectrally constrained waveforms synthesized by the proposed algorithms. Fig. 6 shows the objective values of the synthesized waveforms versus CPU time, where a licensed communication system operates in the (normalized) frequency band $[0.7, 0.8]$, the maximum allowed interference on the communication band is $E_I = 0.05$, and we initialize the proposed algorithms with the scaled eigenvector associated with the smallest eigenvalue of \mathbf{R}_I . To tackle the spectrally constrained quadratic programming problem in (46), we apply the ADMM algorithm proposed in Subsection IV-C and compare it with the FPP-SCA algorithm proposed in [38]. In the ADMM algorithm, we set $\rho = 1$. In the FPP-SCA algorithm, the penalty parameter is 10. In addition, we plot the objective values associated with the energy-constrained waveform as a benchmark. We can observe the convergence of the objective values for all the cases. Moreover, compared with the energy-constrained waveforms, the additional spectral constraint on the waveform results in insignificant performance loss. Furthermore, the application of the proposed ADMM algorithm results in much faster convergence than

that of the FPP-SCA algorithm. This is due to the lower per-iteration computational complexity of the ADMM algorithm ($O(L^3)$) than that of the FPP-SCA algorithm ($O(L^{3.5})$). Fig. 7 shows the ESDs of the synthesized spectral-constrained waveforms at convergence. Note the spectral notch in the communication band (shaded in light gray) and that the interference energy in this band can be controlled ($\leq E_I$). Thus, the waveforms synthesized by the proposed algorithms enable better compatibility with the nearby communication systems.

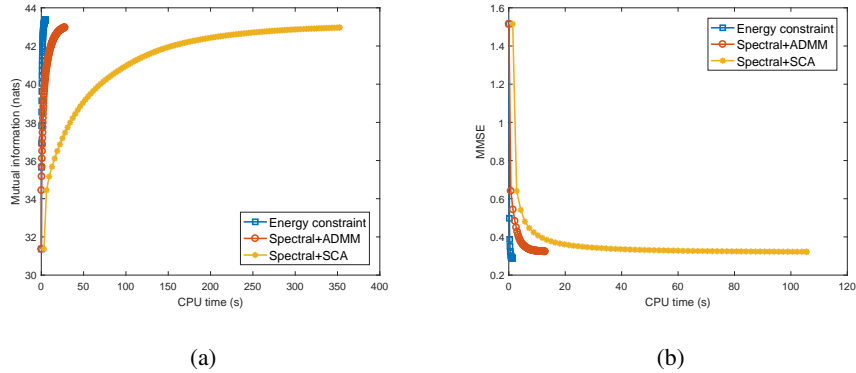


Fig. 6. Convergence of the objective values versus the number of iterations. Spectral constraint. $E_I = 0.05$. (a) Mutual information. (b) MMSE.

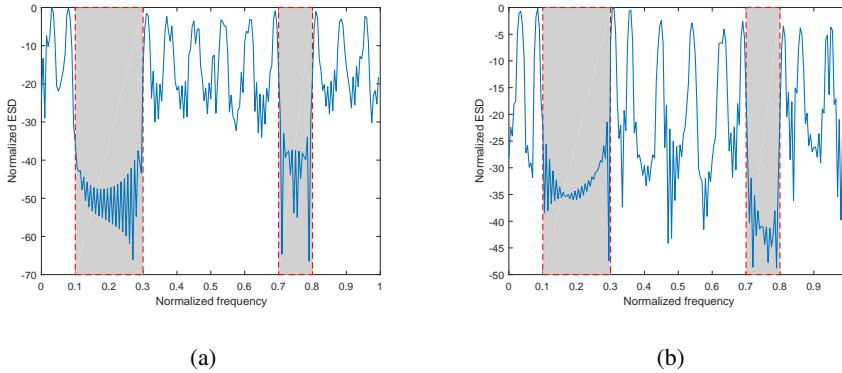


Fig. 7. The ESD of the synthesized spectrally constrained waveform at convergence. $E_I = 0.05$. (a) Mutual information. (b) MMSE.

Fig. 8 compared the MSE of the spectrally constrained waveforms with that of the LFM waveforms for different code lengths, where $e_t = L$, and $E_I = 0.05$. The results indicate that both kinds of waveforms not only have better spectral compatibility than the LFM waveforms, but also achieve smaller MSE. Moreover, for large code length, the performance of the waveform based on maximizing mutual information is almost identical to that the waveform based on minimizing MMSE.

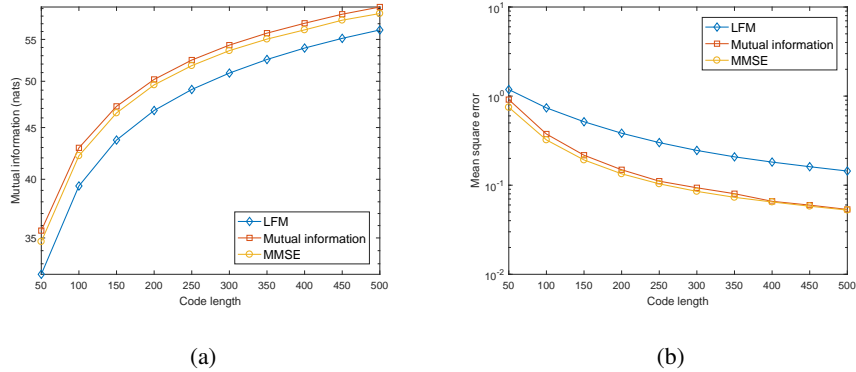


Fig. 8. The performance of the synthesized spectrally constrained waveforms versus code length. $E_1 = 0.05$. (a) Mutual information. (b) MMSE.

C. ZCZ Waveforms

Finally, we show that if the interference in the received signal is dominated by the white noise, and the target covariance matrix is diagonal, the waveforms synthesized by the proposed algorithms will exhibit ZCZ properties. To this end, we set $\mathbf{R}_h = 0.1\mathbf{I}$ and $\mathbf{R}_n = \mathbf{I}$. The convergence of mutual information and MMSE of the constant-modulus waveforms synthesized by the proposed algorithms are shown in Fig. 9(a) and Fig. 9(b), respectively, where we initialize the proposed algorithms by using the LFM waveform, and we set $\varepsilon = 10^{-20}$. The curves in Fig. 9 demonstrate that the objective values converge to the optimal values. Fig. 10 plots the (normalized) auto-correlation function (ACF) of the waveforms synthesized by the proposed algorithms. We can observe that the waveform based on maximizing mutual information has very low correlation sidelobes (lower than about -130 dB) from r_1 to r_{P-1} . For waveform design based on minimizing MMSE, the proposed algorithm converges faster and achieves a lower sidelobe (lower than about -150 dB). Therefore, the synthesized waveforms in this situation have ZCZ properties. In other words, the ZCZ waveforms maximize the mutual information and minimize the MMSE.

VII. CONCLUSION

This paper considered the design of practically constrained waveforms for radar range profiling. Two design metrics were used, i.e., mutual information maximization and MMSE minimization. To tackle the non-convex waveform design problem, we developed an optimization framework based on MM. Due to the ascent property of MM, the proposed algorithms had guaranteed convergence of objective values. Finally, numerical examples demonstrated that the waveforms synthesized by the proposed algorithms were superior to the counterparts.

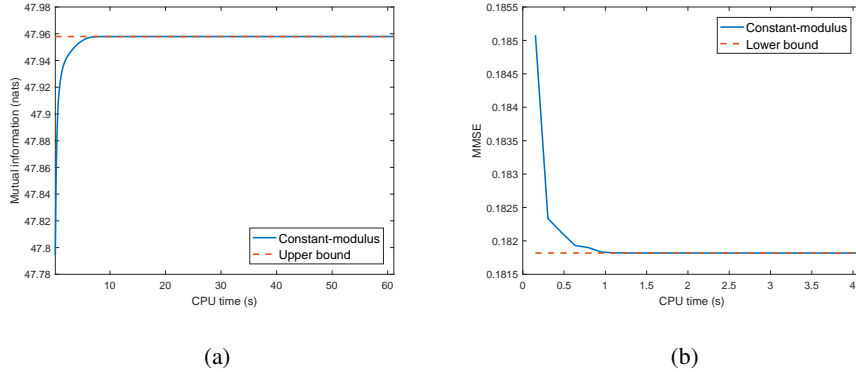


Fig. 9. Convergence of the objective values versus the number of iterations. $\rho = 1$. $\mathbf{R}_h = 0.1\mathbf{I}$. $\mathbf{R}_n = \mathbf{I}$. (a) Mutual information. (b) MMSE.

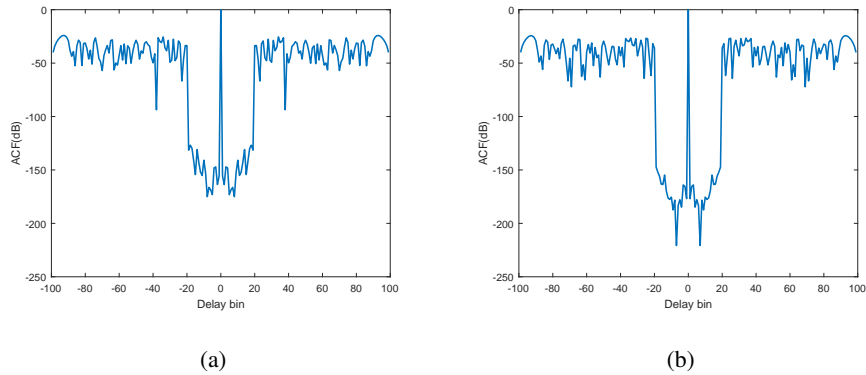


Fig. 10. The ACF of the synthesized constant-modulus waveforms. $\mathbf{R}_h = 0.1\mathbf{I}$. $\mathbf{R}_n = \mathbf{I}$. (a) Mutual information. (b) MMSE.

Possible future research track might concern the extension of the proposed algorithms to design waveforms for radar imaging. In addition, the design of practically constrained waveforms for target recognition/classification might be important (see, e.g., [59], for a recent progress on this topic). Furthermore, the application of the proposed algorithms to polarimetric radar (see, e.g., [14], [15] for some discussions) is left for future work.

APPENDIX A

THE MONOTONICITY OF THE DESIGN METRIC W.R.T. THE TRANSMIT ENERGY

In this appendix, we show that the mutual information is increasing with the waveform energy and the MMSE is decreasing with the waveform energy. To this end, we first prove $f_1(\alpha s) \geq f_1(s)$, where $\alpha \geq 1$.

We note that

$$f_1(\alpha\mathbf{s}) - f_1(\mathbf{s}) = \log \det(\alpha^2 \mathbf{S} \mathbf{R}_h \mathbf{S}^\dagger + \mathbf{R}_n) - \log \det(\mathbf{S} \mathbf{R}_h \mathbf{S}^\dagger + \mathbf{R}_n).$$

Since $\alpha^2 \mathbf{S} \mathbf{R}_h \mathbf{S}^\dagger \succeq \mathbf{S} \mathbf{R}_h \mathbf{S}^\dagger$ and $\log \det(\mathbf{A})$ is an increasing function of $\mathbf{A} \succ \mathbf{0}$, we have $f_1(\alpha\mathbf{s}) - f_1(\mathbf{s}) \geq 0$.

Next we prove that the MMSE is decreasing with the waveform energy. To this end, we rewrite the MMSE as

$$\begin{aligned} & \text{tr}(\mathbf{R}_h - \mathbf{R}_h \mathbf{S}^\dagger (\mathbf{S} \mathbf{R}_h \mathbf{S}^\dagger + \mathbf{R}_n)^{-1} \mathbf{S} \mathbf{R}_h) \\ &= \text{tr} \left((\mathbf{R}_h^{-1} + \mathbf{S}^\dagger \mathbf{R}_n^{-1} \mathbf{S})^{-1} \right). \end{aligned} \quad (66)$$

Since $\alpha^2 \mathbf{S}^\dagger \mathbf{R}_n^{-1} \mathbf{S} \succeq \mathbf{S}^\dagger \mathbf{R}_n^{-1} \mathbf{S}$ and $\text{tr}(\mathbf{A}^{-1})$ is an decreasing function of $\mathbf{A} \succ \mathbf{0}$, we can verify that the MMSE decreases with the transmit energy.

APPENDIX B

PROOF OF PROPOSITION 1

First, it can be checked that the p th column of \mathbf{S} can be written as $\mathbf{E}_p \mathbf{s}$. Thus,

$$\begin{aligned} \text{vec}(\mathbf{S}) &= [(\mathbf{E}_1 \mathbf{s})^T, \dots, (\mathbf{E}_P \mathbf{s})^T]^T \\ &= [\mathbf{E}_1^T, \dots, \mathbf{E}_P^T]^T \mathbf{s} \\ &= \mathbf{E} \mathbf{s}. \end{aligned} \quad (67)$$

Using the fact that $\text{tr}(\mathbf{A}^H \mathbf{B}) = \text{vec}^\dagger(\mathbf{A}) \text{vec}(\mathbf{B})$ [60], we have

$$\begin{aligned} \text{tr}(\mathbf{S}^\dagger \mathbf{G}_k^{21} \mathbf{R}_h^{\frac{1}{2}}) &= \text{vec}^\dagger(\mathbf{S}) \text{vec}(\mathbf{G}_k^{21} \mathbf{R}_h^{\frac{1}{2}}) \\ &= \mathbf{s}^\dagger \mathbf{E}^\dagger \text{vec}(\mathbf{G}_k^{21} \mathbf{R}_h^{\frac{1}{2}}) \\ &= \mathbf{s}^\dagger \mathbf{a}_{I,k}. \end{aligned} \quad (68)$$

In addition, noting that $\text{tr}(\mathbf{ABCD}) = \text{vec}^T(\mathbf{D})(\mathbf{A} \otimes \mathbf{C}^T) \text{vec}(\mathbf{B}^T)$ [60], we can obtain

$$\begin{aligned} \text{tr}(\mathbf{G}_k^{22} \mathbf{S} \mathbf{R}_h \mathbf{S}^\dagger) &= \text{tr}(\mathbf{R}_h \mathbf{S}^\dagger \mathbf{G}_k^{22} \mathbf{S}) \\ &= \text{vec}^T(\mathbf{S})(\mathbf{R}_h \otimes (\mathbf{G}_k^{22})^T) \text{vec}(\mathbf{S}^*) \\ &= \mathbf{s}^T \mathbf{E}^T (\mathbf{R}_h \otimes (\mathbf{G}_k^{22})^T) \mathbf{E}^* \mathbf{s}^* \\ &= \mathbf{s}^\dagger \mathbf{E}^\dagger (\mathbf{R}_h^* \otimes \mathbf{G}_k^{22}) \mathbf{E} \mathbf{s} \\ &= \mathbf{s}^\dagger \mathbf{A}_{I,k} \mathbf{s}, \end{aligned} \quad (69)$$

where the first line holds because $\text{tr}(\mathbf{AB}) = \text{tr}(\mathbf{BA})$, the fourth line follows from that \mathbf{G}_k^{22} and $\mathbf{S} \mathbf{R}_h \mathbf{S}^\dagger$ are both Hermitian, and $\text{tr}(\mathbf{G}_k^{22} \mathbf{S} \mathbf{R}_h \mathbf{S}^\dagger)$ is real-valued.

Combing (68) and (69), we complete the proof.

APPENDIX C

PROOF OF LEMMA 1

According to [50], the epigraph of $\psi(\mathbf{A}, \mathbf{B})$ is defined by

$$\text{epi}(\psi) = \left\{ (\mathbf{A}, \mathbf{B}, t) \mid \text{tr}(\mathbf{A}^\dagger \mathbf{B}^{-1} \mathbf{A}) \leq t \right\}. \quad (70)$$

Note that $\text{tr}(\mathbf{A}^\dagger \mathbf{B}^{-1} \mathbf{A}) \leq t$ is equivalent to $\{\text{tr}(\mathbf{Y}) \leq t, \mathbf{A}^\dagger \mathbf{B}^{-1} \mathbf{A} \succeq \mathbf{Y}, \mathbf{Y} \succeq \mathbf{0}\}$. Thus, $\text{epi}(\psi)$ can be rewritten as

$$\text{epi}(\psi) = \left\{ (\mathbf{A}, \mathbf{B}, t) \mid \exists \mathbf{Y} \succeq \mathbf{0}, \begin{bmatrix} \mathbf{B} & \mathbf{A} \\ \mathbf{A}^\dagger & \mathbf{Y} \end{bmatrix} \succeq \mathbf{0}, \text{tr}(\mathbf{Y}) \leq t \right\}.$$

It is easy to check that $\text{epi}(\psi)$ is convex. Therefore, $\psi(\mathbf{A}, \mathbf{B})$ is a convex function of the matrix pair (\mathbf{A}, \mathbf{B}) (namely, jointly convex). Using the fact that convex functions are minorized by their supporting hyperplanes, we have

$$\begin{aligned} \text{tr}(\mathbf{A}^\dagger \mathbf{B}^{-1} \mathbf{A}) &\geq \text{tr}(\mathbf{A}_k^\dagger \mathbf{B}_k^{-1} \mathbf{A}_k) + 2\text{Re}(\text{tr}(\mathbf{A}_k^\dagger \mathbf{B}_k^{-1} (\mathbf{A} - \mathbf{A}_k))) \\ &\quad - \text{tr}(\mathbf{B}_k^{-1} \mathbf{A}_k \mathbf{A}_k^\dagger \mathbf{B}_k^{-1} (\mathbf{B} - \mathbf{B}_k)) \\ &= 2\text{Re}(\text{tr}(\mathbf{A}_k^\dagger \mathbf{B}_k^{-1} \mathbf{A})) - \text{tr}(\mathbf{B}_k^{-1} \mathbf{A}_k \mathbf{A}_k^\dagger \mathbf{B}_k^{-1} \mathbf{B}), \end{aligned}$$

where $(\mathbf{A}_k^\dagger \mathbf{B}_k^{-1}, -\mathbf{B}_k^{-1} \mathbf{A}_k \mathbf{A}_k^\dagger \mathbf{B}_k^{-1})$ is the gradient of $\psi(\mathbf{A}, \mathbf{B})$ at $(\mathbf{A}_k, \mathbf{B}_k)$ (which can be shown using the results from [51], [61]).

An alternative proof without using convexity is by noting that (since $\mathbf{B} \succ \mathbf{0}$)

$$(\mathbf{B}^{-1} \mathbf{A} - \mathbf{B}_k^{-1} \mathbf{A}_k)^\dagger \mathbf{B} (\mathbf{B}^{-1} \mathbf{A} - \mathbf{B}_k^{-1} \mathbf{A}_k) \succeq \mathbf{0}. \quad (71)$$

Thus,

$$\text{tr}[(\mathbf{B}^{-1} \mathbf{A} - \mathbf{B}_k^{-1} \mathbf{A}_k)^\dagger \mathbf{B} (\mathbf{B}^{-1} \mathbf{A} - \mathbf{B}_k^{-1} \mathbf{A}_k)] \geq 0. \quad (72)$$

After some algebraic manipulations, we complete the proof.

APPENDIX D

PROOF OF NEGATIVE SEMI-DEFINITENESS OF $\mathbf{A}_{I,k}$ AND $\mathbf{A}_{E,k}$

To prove that $\mathbf{A}_{I,k}$ is negative semi-definite, it is sufficient to prove that $\mathbf{R}_h^* \otimes \mathbf{G}_k^{22}$ is negative semi-definite. Note that $\mathbf{R}_h \succ \mathbf{0}$. In addition, since $\mathbf{R}_{s,k} \succeq \mathbf{R}_n$, we have $\mathbf{G}_k^{22} = \mathbf{R}_{s,k}^{-1} - \mathbf{R}_n^{-1} \preceq \mathbf{0}$. Thus, $\mathbf{R}_h^* \otimes \mathbf{G}_k^{22} \preceq \mathbf{0}$. Similarly, to identify the negative semi-definiteness of $\mathbf{A}_{E,k}$, it is sufficient to prove that $\mathbf{R}_h^* \otimes \mathbf{T}_k \succeq \mathbf{0}$. Note that $\mathbf{T}_k = \mathbf{R}_{s,k}^{-1} \mathbf{S}_k \mathbf{R}_h^2 \mathbf{S}_k^\dagger \mathbf{R}_{s,k}^{-1} \succeq \mathbf{0}$. Thus, $\mathbf{A}_{E,k}$ is negative semi-definite.

REFERENCES

- [1] D. R. Wehner, *High resolution radar*. Norwood: Artech House, 1995.
- [2] P. Tait, *Introduction to radar target recognition*. London: The Institution of Electronic Technology, 2005.
- [3] N. Levanon, "Cross-correlation of long binary signals with longer mismatched filters," *IEE Proceedings-Radar, Sonar and Navigation*, vol. 152, no. 6, pp. 377–382, 2005.
- [4] P. Stoica, J. Li, and M. Xue, "Transmit codes and receive filters for radar," *IEEE Signal Process. Mag.*, vol. 25, no. 6, pp. 94–109, 2008.
- [5] S. M. H. Song, W. M. Kim, P. Dongwook, and K. Young-Sik, "Estimation theoretic approach for radar pulse compression processing and its optimal codes," *Electronics Letters*, vol. 36, no. 3, pp. 250–252, 2000.
- [6] S. D. Blunt and K. Gerlach, "Adaptive pulse compression via MMSE estimation," *IEEE Trans. Aerosp. Electron. Syst.*, vol. 42, no. 2, pp. 572–584, 2006.
- [7] H. Kikuchi, E. Yoshikawa, T. Ushio, F. Mizutani, and M. Wada, "Adaptive pulse compression technique for X-Band phased array weather radar," *IEEE Geoscience and Remote Sensing Letters*, vol. 14, no. 10, pp. 1810–1814, 2017.
- [8] T. Yardibi, J. Li, P. Stoica, M. Xue, and A. B. Baggeroer, "Source localization and sensing: A nonparametric iterative adaptive approach based on weighted least squares," *IEEE Trans. Aerosp. Electron. Syst.*, vol. 46, no. 1, pp. 425–443, 2010.
- [9] H. He, J. Li, and P. Stoica, *Waveform design for active sensing systems: a computational approach*. Cambridge University Press, 2012.
- [10] F. Gini, A. De Maio, and L. Patton, *Waveform design and diversity for advanced radar systems*. London: Institution of engineering and technology, 2012.
- [11] G. Cui, A. De Maio, A. Farina, and J. Li, *Radar Waveform Design Based on Optimization Theory*. London: SciTech Publishing, 2020.
- [12] P. Stoica, H. He, and J. Li, "New algorithms for designing unimodular sequences with good correlation properties," *IEEE Trans. Signal Process.*, vol. 57, no. 4, pp. 1415–1425, 2009.
- [13] J. Song, P. Babu, and D. P. Palomar, "Optimization methods for designing sequences with low autocorrelation sidelobes," *IEEE Trans. Signal Process.*, vol. 63, no. 15, pp. 3998–4009, 2015.
- [14] D. A. Garren, A. Odom, M. Osborn, J. S. Goldstein, S. Pillai, and J. Guerci, "Full-polarization matched-illumination for target detection and identification," *IEEE Trans. Aerosp. Electron. Syst.*, vol. 38, no. 3, pp. 824–837, 2002.
- [15] X. Cheng, A. Aubry, D. Ciuonzo, A. D. Maio, and X. Wang, "Robust waveform and filter bank design of polarimetric radar," *IEEE Trans. Aerosp. Electron. Syst.*, vol. 53, no. 1, pp. 370–384, 2017.
- [16] D. Ciuonzo, A. De Maio, G. Foglia, and M. Piezzo, "Intrapulse radar-embedded communications via multiobjective optimization," *IEEE Trans. Aerosp. Electron. Syst.*, vol. 51, no. 4, pp. 2960–2974, 2015.
- [17] B. Tang and J. Tang, "Joint design of transmit waveforms and receive filters for MIMO radar space-time adaptive processing," *IEEE Trans. Signal Process.*, vol. 64, no. 18, pp. 4707–4722, 2016.
- [18] B. Tang, J. Tuck, and P. Stoica, "Polyphase waveform design for MIMO radar space time adaptive processing," *IEEE Trans. Signal Process.*, vol. 68, pp. 2143–2154, 2020.
- [19] M. R. Bell, "Information theory and radar waveform design," *IEEE Trans. Inf. Theory*, vol. 39, no. 5, pp. 1578–1597, 1993.
- [20] A. Leshem, O. Naparstek, and A. Nehorai, "Information theoretic adaptive radar waveform design for multiple extended targets," *IEEE Journal of Selected Topics in Signal Processing*, vol. 1, no. 1, pp. 42–55, 2007.

- [21] R. A. Romero, J. Bae, and N. A. Goodman, "Theory and application of SNR and mutual information matched illumination waveforms," *IEEE Trans. Aerosp. Electron. Syst.*, vol. 47, no. 2, pp. 912–927, 2011.
- [22] K.-W. Huang, M. Bicá, U. Mitra, and V. Koivunen, "Radar waveform design in spectrum sharing environment: Coexistence and cognition," in *IEEE Radar Conference (RadarCon)*, 2015, pp. 1698–1703.
- [23] M. Bicá, K.-W. Huang, V. Koivunen, and U. Mitra, "Mutual information based radar waveform design for joint radar and cellular communication systems," in *IEEE International Conference on Acoustics, Speech and Signal Processing (ICASSP)*. IEEE, 2016, pp. 3671–3675.
- [24] R. Palamá, H. Griffiths, and F. Watson, "Joint dynamic spectrum access and target-matched illumination for cognitive radar," *IET Radar, Sonar & Navigation*, vol. 13, no. 5, pp. 750–759, 2019.
- [25] B. Tang and J. Li, "Spectrally constrained MIMO radar waveform design based on mutual information," *IEEE Trans. Signal Process.*, vol. 67, no. 3, pp. 821–834, 2019.
- [26] S. M. Karbasi, A. Aubry, A. De Maio, and M. H. Bastani, "Robust transmit code and receive filter design for extended targets in clutter," *IEEE Trans. Signal Process.*, vol. 63, no. 8, pp. 1965–1976, 2015.
- [27] B. Tang and J. Tang, "Robust waveform design of wideband cognitive radar for extended target detection," in *IEEE International Conference on Acoustics, Speech and Signal Processing (ICASSP)*, 2016, Conference Proceedings, pp. 3096–3100.
- [28] S. Z. Gurbuz, H. D. Griffiths, A. Charlish, M. Rangaswamy, M. S. Greco, and K. Bell, "An overview of cognitive radar: Past, present, and future," *IEEE Aerosp. Electron. Syst. Mag.*, vol. 34, no. 12, pp. 6–18, 2019.
- [29] C. P. Horne, A. M. Jones, G. E. Smith, and H. D. Griffiths, "Fast fully adaptive signalling for target matching," *IEEE Aerosp. Electron. Syst. Mag.*, vol. 35, no. 6, pp. 46–62, 2020.
- [30] G. E. Smith, Z. Cammenga, A. Mitchell, K. L. Bell, J. Johnson, M. Rangaswamy, and C. Baker, "Experiments with cognitive radar," *IEEE Aerosp. Electron. Syst. Mag.*, vol. 31, no. 12, pp. 34–46, 2016.
- [31] T. M. Cover and J. A. Thomas, *Elements of information theory*. New Jersey: John Wiley & Sons, 2012.
- [32] S. M. Kay, *Fundamentals of Statistical Signal Processing: Estimation Theory*. New Jersey: Prentice Hall, 1993.
- [33] R. A. Horn and C. R. Johnson, *Matrix analysis*. Cambridge: Cambridge University Press, 1990.
- [34] A. De Maio, S. De Nicola, Y. Huang, Z.-Q. Luo, and S. Zhang, "Design of phase codes for radar performance optimization with a similarity constraint," *IEEE Trans. Signal Process.*, vol. 57, no. 2, pp. 610–621, 2009.
- [35] A. De Maio, Y. Huang, M. Piezzo, S. Zhang, and A. Farina, "Design of optimized radar codes with a peak to average power ratio constraint," *IEEE Trans. Signal Process.*, vol. 59, no. 6, pp. 2683–2697, 2011.
- [36] P. Stoica, H. He, and J. Li, "Optimization of the receive filter and transmit sequence for active sensing," *IEEE Trans. Signal Process.*, vol. 60, no. 4, pp. 1730–1740, 2012.
- [37] M. Soltanalian, B. Tang, J. Li, and P. Stoica, "Joint design of the receive filter and transmit sequence for active sensing," *IEEE Signal Processing Letters*, vol. 20, no. 5, pp. 423–426, 2013.
- [38] L. Wu, P. Babu, and D. P. Palomar, "Transmit waveform/receive filter design for MIMO radar with multiple waveform constraints," *IEEE Trans. Signal Process.*, vol. 66, no. 6, pp. 1526–1540, 2018.
- [39] A. Aubry, A. D. Maio, M. A. Govoni, and L. Martino, "On the design of multi-spectrally constrained constant modulus radar signals," *IEEE Trans. Signal Process.*, vol. 68, pp. 2231–2243, 2020.
- [40] B. Tang and P. Stoica, "Information-theoretic waveform design for MIMO radar detection in range-spread clutter," *Signal Processing*, vol. 182, p. 107961, 2021.
- [41] H. Griffiths, L. Cohen, S. Watts, E. Mokole, C. Baker, M. Wicks, and S. Blunt, "Radar spectrum engineering and management: technical and regulatory issues," *Proceedings of the IEEE*, vol. 103, no. 1, pp. 85–102, 2015.

- [42] M. Bockmair, C. Fischer, M. Letsche-Nuesseler, C. Neumann, M. Schikorr, and M. Steck, "Cognitive radar principles for defence and security applications," *IEEE Aerosp. Electron. Syst. Mag.*, vol. 34, no. 12, pp. 20–29, 2019.
- [43] V. Carotenuto, A. Aubry, A. D. Maio, N. Pasquino, and A. Farina, "Assessing agile spectrum management for cognitive radar on measured data," *IEEE Aerosp. Electron. Syst. Mag.*, vol. 35, no. 6, pp. 20–32, 2020.
- [44] J. Yang, A. Aubry, A. De Maio, X. Yu, and G. Cui, "Design of constant modulus discrete phase radar waveforms subject to multi-spectral constraints," *IEEE Signal Processing Letters*, vol. 27, pp. 875–879, 2020.
- [45] A. Aubry, A. De Maio, M. Piezzo, and A. Farina, "Radar waveform design in a spectrally crowded environment via nonconvex quadratic optimization," *IEEE Trans. Aerosp. Electron. Syst.*, vol. 50, no. 2, pp. 1138–1152, 2014.
- [46] A. Aubry, V. Carotenuto, A. De Maio, A. Farina, and L. Pallotta, "Optimization theory-based radar waveform design for spectrally dense environments," *IEEE Aerosp. Electron. Syst. Mag.*, vol. 31, no. 12, pp. 14–25, 2016.
- [47] D. R. Hunter and K. Lange, "A tutorial on MM algorithms," *The American Statistician*, vol. 58, no. 1, pp. 30–37, 2004.
- [48] Y. Sun, P. Babu, and D. P. Palomar, "Majorization-minimization algorithms in signal processing, communications, and machine learning," *IEEE Trans. Signal Process.*, vol. 65, no. 3, pp. 794–816, 2017.
- [49] B. Tang, Y. Zhang, and J. Tang, "An efficient minorization maximization approach for MIMO radar waveform optimization via relative entropy," *IEEE Trans. Signal Process.*, vol. 66, no. 2, pp. 400–411, 2018.
- [50] S. Boyd and L. Vandenberghe, *Convex optimization*. Cambridge: Cambridge University Press, 2004.
- [51] A. Hjørungnes and D. Gesbert, "Complex-valued matrix differentiation: Techniques and key results," *IEEE Trans. Signal Process.*, vol. 55, no. 6, pp. 2740–2746, 2007.
- [52] J. A. Tropp, I. S. Dhillon, R. W. Heath, and T. Strohmer, "Designing structured tight frames via an alternating projection method," *IEEE Trans. Inf. Theory*, vol. 51, no. 1, pp. 188–209, 2005.
- [53] W. Ai, Y. Huang, and S. Zhang, "New results on hermitian matrix rank-one decomposition," *Mathematical programming*, vol. 128, no. 1-2, pp. 253–283, 2011.
- [54] S. Boyd, N. Parikh, E. Chu, B. Peleato, and J. Eckstein, "Distributed optimization and statistical learning via the alternating direction method of multipliers," *Foundations and Trends® in Machine Learning*, vol. 3, no. 1, pp. 1–122, 2011.
- [55] B. Tang, J. Li, and J. Liang, "Alternating direction method of multipliers for radar waveform design in spectrally crowded environments," *Signal Processing*, vol. 142, pp. 398–402, 2018.
- [56] J. Li, J. R. Guerci, and L. Xu, "Signal waveform's optimal-under-restriction design for active sensing," *IEEE Signal Processing Letters*, vol. 13, no. 9, pp. 565–568, 2006.
- [57] P. Z. Fan, N. Suehiro, N. Kuroyanagi, and X. M. Deng, "Class of binary sequences with zero correlation zone," *Electronics Letters*, vol. 35, no. 10, pp. 777–779, 1999.
- [58] Y. Yang and R. S. Blum, "MIMO radar waveform design based on mutual information and minimum mean-square error estimation," *IEEE Trans. Aerosp. Electron. Syst.*, vol. 43, no. 1, pp. 330–343, 2007.
- [59] Y. Gu and N. A. Goodman, "Information-theoretic waveform design for Gaussian mixture radar target profiling," *IEEE Trans. Aerosp. Electron. Syst.*, vol. 55, no. 3, pp. 1528–1536, 2019.
- [60] D. S. Bernstein, *Matrix mathematics: theory, facts, and formulas*. Princeton University Press, 2009.
- [61] J. V. Burke and T. Hoheisel, "Matrix support functionals for inverse problems, regularization, and learning," *SIAM Journal on Optimization*, vol. 25, no. 2, pp. 1135–1159, 2015.